

Macroscopic effects of localised measurements in jammed states of quantum spin chains

Kemal Bidzhiev, Maurizio Fagotti,* and Lenart Zadnik
Université Paris-Saclay, CNRS, LPTMS, 91405, Orsay, France

A quantum jammed state can be seen as a state where the phase space available to particles shrinks to zero, an interpretation quite accurate in integrable systems, where stable quasiparticles scatter elastically. We consider the integrable dual folded XXZ model, which is equivalent to the XXZ model in the limit of large anisotropy. We perform a jamming-breaking localised measurement in a jammed state. We find that jamming is locally restored, but local observables exhibit nontrivial time evolution on macroscopic, ballistic scales, without ever relaxing back to their initial values.

Introduction. Recent remarkable progress in quantum information science owes much to the advancement of cold-atom and trapped-ion setups [1–4]. These have become so refined [5–8] to allow for the design of so-called “quantum simulators” [9]. Understanding the effects of perturbations and measurements has always been crucial in this regard, be it due to the role of perturbations in the decoherence process, or the one of measurements in simulation protocols [10]. Integrable [11–14] and generic [15–20] quantum circuits are potentially useful in this endeavour: they allow for some degree of exact treatment [21–24] and benefit experimental realisation [25, 26].

Localised measurements can be viewed as a type of “quantum quench”, i.e., the non-equilibrium dynamics induced by a sudden perturbation, studied in the last decades especially in the context of relaxation in quantum many-body systems (see [27] and articles therein). Such perturbations break the homogeneity of the system, making its study challenging. In integrable models the most effective large-scale description of the dynamics in the presence of inhomogeneities is arguably the so-called “generalised hydrodynamics” (GHD) [28–30]. Although GHD correctly predicts the large-scale dynamics of local observables in numerous quench protocols (e.g., in the two-temperatures scenario), the information provided by the theory is sometimes incomplete. The first example of this kind was exhibited in Ref. [31], considering the massive Heisenberg model: the ingredients of GHD are blind to observables that are odd under spin flip, entailing the inclusion of an additional independent continuity equation. An even more striking example was considered in Refs [32–36], in which GHD keeps a symmetry that is instead broken in the thermodynamic limit: observables not respecting that symmetry are affected by a class of localised perturbations at arbitrarily long times and large distances from the inhomogeneity.

In this Letter we study the effect of a localised projective measurement in a quantum jammed state. To this end we consider the so-called “wing-flap protocol” introduced in Ref. [37] to provide insight into the quantum information scrambling: the system is prepared in a state ρ ; an observable O is measured; the system is let to evolve with $-H$ for a time t ; a “wing-flap” perturbation

W is applied; the system is let to evolve with H for a time t ; O is measured again. A similar scheme was recently studied in Ref. [38], where W corresponded to a “blind” local projective quantum measurement at the position of O , in which neither the outcome of the measurement, nor the measured operator are known. In addition, the last step of the above protocol was upgraded to a quantum state tomography in order to recover the local state after the second step. Under some assumptions Ref. [38] showed that, if H describes a generic system, the local state can be recovered with a limited amount of effort.

For our purpose the wing-flap protocol is modified as follows. The system is prepared in a low-entangled stationary state, which, we assume, is also an eigenstate of the operator measured by Alice (as shown later, this is easily realisable in our system). We then go back in time (a trivial step, since the state is stationary) considering an alternative history in which, at some unknown but fixed ancient time, Bob had performed an unknown projective quantum measurement at an unknown but fixed large distance from Alice. Returning to an alternative present, following Ref. [38] we wonder whether Alice can still recover the information she had without Bob’s intervention.

Generally, in a shift invariant quantum spin chain the distant Bob’s measurement is not expected to have any effect on Alice’s subsystem. In particular, Ref. [39] showed that, in noninteracting spin chains, relaxation to a Generalised Gibbs ensemble (GGE) is not compromised by a localised perturbation. In our setting this implies that, at late times, the effect of Bob’s measurement on a finite subsystem fades away. We are not aware of any physical argument against the generalisation of this result to interacting integrable systems. Indeed, this conclusion is supported by numerical investigations, which generally show the irrelevance of localised perturbations on the state after long-enough time. Consider, for example, the numerical tests of the generalised hydrodynamic predictions of time evolution after two different states are joined together [40]. The tests always differ in the way the states are joined, nevertheless the asymptotic behaviours at large times match. In generic systems scrambling is even more pronounced, so a very distant quantum

measurement in a low-entangled stationary state is not expected to have visible effects however large the time is. Incidentally, even if the state weren't stationary and Bob measured an observable in Alice's subsystem, Alice would be able to recover the original local state [38].

Here we apply this protocol to the dual folded XXZ spin-1/2 chain, which belongs to a class of effective models emerging in strong coupling limits of spin chains [41]. It corresponds to a special point of the two-component Bariev model [42] and is described by the Hamiltonian

$$H = J \sum_{\ell} (\sigma_{\ell}^x \sigma_{\ell+2}^x + \sigma_{\ell}^y \sigma_{\ell+2}^y) \frac{\mathbb{1} - \sigma_{\ell+1}^z}{2}. \quad (1)$$

The model can be solved exactly by introducing two species of particles associated with spins up on either even or odd sites [41] (see also [43]). The solution is based on the observation that the unique nontrivial effect of H corresponds to moving a spin up by two sites when it is adjacent to two spins down $|\uparrow\downarrow\downarrow\rangle \leftrightarrow |\downarrow\downarrow\uparrow\rangle$. The same observation also implies the existence of an exponentially large number of states with clustering properties in which the aforementioned particles are stacked together and cannot move. These are the states that we call jammed.

We report a striking exception to the empirical rule that a distant localised perturbation in a low-entangled state of a quantum many-body system described by a translationally invariant Hamiltonian does not have visible effects at infinitely large times and distances. To the best of our knowledge, only one exception has been reported so far and it concerns systems prepared in the ground state when a discrete symmetry is spontaneously broken [32–36]. Similarly, we consider an initial state that breaks the conserved charges that completely characterise a basis of energy eigenstates, but, differently, our initial state belongs to an *exponentially* large degenerate sector. We will show that, in the limit of large time, the jammed sector is asymptotically stable under the wing-flap protocol. Quite exceptionally, we also demonstrate that the measurement results in a macroscopic change of the spin profiles on ballistic scales, namely its effect does not fade away at large times, the expectation values of local observables instead approaching nontrivial functions of the ratio between distance and time.

Quantum jamming. Our discussion is specialised to the sector spanned by states $|\Phi\rangle$ satisfying the *jamming condition*

$$\mathcal{P}_{\downarrow\downarrow}(\ell) \equiv \langle \Phi | \frac{\mathbb{1} - \sigma_{\ell}^z}{2} \frac{\mathbb{1} - \sigma_{\ell+1}^z}{2} | \Phi \rangle = 0, \quad \forall \ell. \quad (2)$$

Any such a state is an eigenstate of H with zero energy and is *jammed* [41, 44, 45]. Jammed states are special since they can break the two-site shift invariance of the complete set of charges exhibited in Ref. [41]. This is possible because the spectrum has huge degeneracies associated with hidden symmetries, which have been shown,

for example, to play a key role in the quench dynamics within the non-interacting sectors of the model [46].

The simplest basis of the jammed sector consists of product states that are eigenstates of $\{\sigma_{\ell}^z\}$, but one can easily construct states with any entanglement entropy density up to $\frac{1}{2} \log 2$. For example, if o denotes the sublattice of odd sites and e the one of even sites, the state $|\uparrow \dots \uparrow\rangle_o \otimes |\psi\rangle_e$ is jammed and the entanglement entropy of a spin block is half of that in the state $|\psi\rangle$. Particularly interesting are $(2n)$ -site shift invariant jammed product states that are not eigenstates of $\{\sigma_{\ell}^z\}$, e.g.,

$$|\mathcal{L}_n\rangle = e^{i \frac{\pi}{2n} \sum_j j \sigma_j^z} |\uparrow\leftarrow \dots \uparrow\leftarrow\rangle. \quad (3)$$

This family of stationary states breaks the $U(1)$ symmetry generated by $\sum_{\ell} \sigma_{\ell}^z$ and, for $n > 1$, also the 2-site shift invariance of the model's charges. Such states belong to the fully interacting sector of the model, which is characterised by the presence of spins up on both even and odd positions [41].

The jammed sector is invariant under measurements of operators that commute with all elements of the set $\{\sigma_{\ell}^z\}$. Note instead that measuring other observables generally results in leaving the sector.

Locally quasi-jammed states. Criterion (2) can be modified to define states that are jammed asymptotically in some scaling limit $\xi \rightarrow \infty$, with $\ell = \ell(\xi)$, $t = t(\xi)$, where ξ is the typical scale of the inhomogeneity. We can then envisage inhomogeneous states satisfying

$$\lim_{\xi \rightarrow \infty} \langle \Phi_{t(\xi)} | \frac{\mathbb{1} - \sigma_{\ell(\xi)}^z}{2} \frac{\mathbb{1} - \sigma_{\ell(\xi)+1}^z}{2} | \Phi_{t(\xi)} \rangle = 0, \quad \forall \ell. \quad (4)$$

We call them locally quasi-jammed states (LQJS), by analogy with the terminology used for the locally quasi-stationary states (LQSS) that evolve according to generalised hydrodynamics [28]. A difference between an LQSS and an LQJS is that, in the scaling limit, only the former is forced to locally respect the symmetries of a complete set of charges.

We will focus on initial states belonging to the family $|\mathcal{L}_n\rangle$ and, for the sake of simplicity, assume Alice to measure $\cos(\frac{j\pi}{n})\sigma_j^x - \sin(\frac{j\pi}{n})\sigma_j^y$, with j even, so that $|\mathcal{L}_n\rangle$ is not affected by the measurement. The state after Alice's measurement will then be of the form $|\Phi\rangle = |\uparrow \dots \uparrow\rangle_o \otimes |\varphi_0\rangle_e$. Let then Bob be in an odd position $2\ell' - 1$ and perform a blind measurement of the spin. Since the spin is up before the measurement, the density matrix after the measurement, $\rho(0)$, will commute with $\sigma_{2\ell'-1}^z$; in particular it reads

$$\rho(0) = \frac{2}{3} |\Phi\rangle \langle \Phi| + \frac{1}{3} \sigma_{2\ell'-1}^x |\Phi\rangle \langle \Phi| \sigma_{2\ell'-1}^x. \quad (5)$$

The coefficients 2/3 and 1/3 come from considering a (blind) projective measurement – see the Supplementary material (SM) [47]. Nevertheless, the structure of the

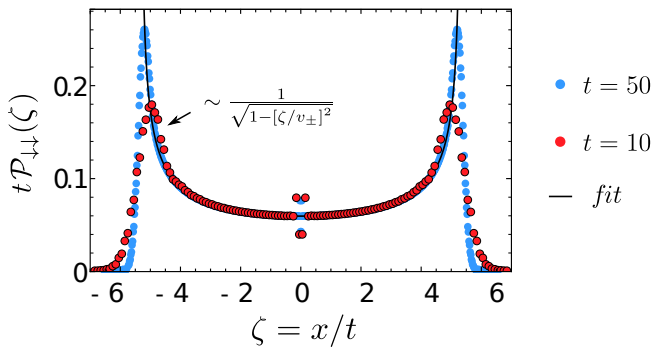


FIG. 1. Profile of the rescaled jamming criterion $t\mathcal{P}_{\downarrow\downarrow}(x/t)$ at times $t = 10, 50$ after the flip of the central spin up (in an odd position) of the state $|\mathcal{L}_1\rangle = |\uparrow\leftarrow\uparrow\leftarrow\dots\rangle$. The data inside the light cone are in excellent agreement with conjecture (14). The jamming condition is locally restored as $\mathcal{P}_{\downarrow\downarrow}(x/t) \sim 1/t$.

density matrix would remain the same also under more general measurement protocols. A local measurement can break condition (2) only locally and, because the Hamiltonian effectively moves the defect as in a classical random walk ($|\uparrow\downarrow\rangle \leftrightarrow |\downarrow\uparrow\rangle$), it is reasonable to expect diffusive behaviour that will make (2) valid in the limit of large time. We can then expect an LQJS to emerge, namely a state where (4) holds. This expectation is supported by our numerical investigation – see Fig. 1.

Notwithstanding the initial state being shift invariant by a finite number of sites, Bob’s measurement locally breaks that symmetry. We find that, while shift invariance is locally restored, it remains globally broken, as in the systems that can be described by generalised hydrodynamics. Contrary to the latter case, however, the two-site shift invariance, which is a symmetry of a complete set of local conservation laws, is generally not restored, even locally. Figure 2, for instance, shows that the xy -plane spin profiles remain staggered on the sublattice of even sites, however long the time after the initial perturbation to the state $|\mathcal{L}_2\rangle$ is: only 4-site shift invariance is locally restored. This property is shared with non-abelian integrable systems like the quantum XY model, where the late time behaviour is generally not captured by a macro-state characterised by the complete set of one-site shift invariant charges [46].

Dynamics after a local spin flip. Since $|\Phi\rangle$ is an eigenstate, the time evolution of (5) can be immediately deduced from that of

$$|\Psi(0)\rangle = \sigma_{2\ell'-1}^x |\Phi\rangle \equiv (\sigma_0^x |\uparrow\dots\uparrow\rangle)_o \otimes |\varphi_0\rangle_e, \quad (6)$$

where, without loss of generality, we have set $\ell' = 0$. The state at time t can then be represented as follows

$$|\Psi(t)\rangle = \sum_n (\sigma_n^x |\uparrow\dots\uparrow\rangle)_o \otimes |\varphi_n(t)\rangle_e, \quad (7)$$

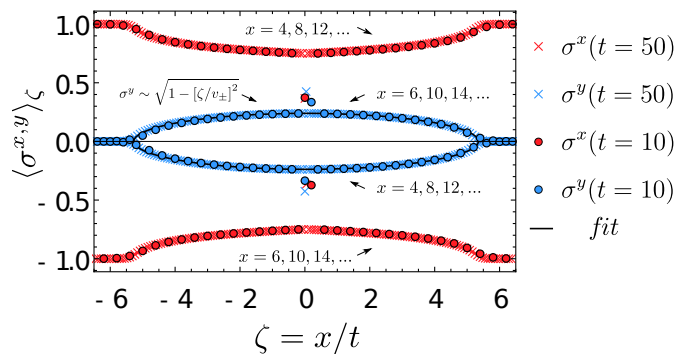


FIG. 2. Spin profiles $\langle\sigma^x\rangle_{\zeta}$ (red) and $\langle\sigma^y\rangle_{\zeta}$ (blue) at times $t = 10, 50$ after having flipped the central spin up (in an odd position) of the state $|\mathcal{L}_2\rangle = |\uparrow\leftarrow\uparrow\rightarrow\dots\rangle$. Nontrivial profiles emerge on *even* sites, whereas spins on odd positions relax to their original values along the z direction. The data for $\langle\sigma^y\rangle_{\zeta}$ are in excellent agreement with conjecture (14).

where the unnormalized wave functions $|\varphi_n(t)\rangle_e$ of spins on the sublattice of even sites satisfy

$$i\partial_{Jt} |\varphi_n(t)\rangle = K_{n-1,n} |\varphi_n(t)\rangle + (\mathbb{1} - \sigma_{n-1}^z) |\varphi_{n-1}(t)\rangle + (\mathbb{1} - \sigma_n^z) |\varphi_{n+1}(t)\rangle \quad (8)$$

with $|\varphi_n(0)\rangle = \delta_{n,0} |\varphi_0\rangle$. Here $K_{n-1,n} = \sigma_{n-1}^x \sigma_n^x + \sigma_{n-1}^y \sigma_n^y$. Note that this is a system of $\log_2 \sqrt{D}$ equations for $|\varphi_n(t)\rangle$, which are states belonging to subspaces of size \sqrt{D} , where D denotes the size of the Hilbert space.

The dynamical equation (8) is block-diagonal in the Fourier space defined by

$$|\tilde{\varphi}_P(t)\rangle = \sum_n e^{inP} \Pi^{-n} |\varphi_n(t)\rangle, \quad (9)$$

where Π is the 1-site shift operator on the sublattice, such that $\Pi^{-1} = \Pi^\dagger$ and $\Pi(O_\ell)_{o(e)} \Pi^\dagger = (O_{\ell+1})_{o(e)}$. Specifically, we find

$$|\tilde{\varphi}_P(t)\rangle = e^{-i\tilde{H}(P)t} |\varphi_0\rangle, \quad (10)$$

where the independent time evolutions labelled by P are generated by

$$\tilde{H}(P) = J [K_{-1,0} + (e^{-iP} \Pi (\mathbb{1} - \sigma_{-1}^z) + h.c.)]. \quad (11)$$

Since Π is a sublattice shift, P is the eigenvalue of the momentum generating the two-site shifts on the full lattice. Indeed, denoting by U the map $|\varphi_n(t)\rangle \mapsto \Pi |\varphi_{n-1}(t)\rangle$ we find $U |\tilde{\varphi}_P(t)\rangle = e^{iP} |\tilde{\varphi}_P(t)\rangle$.

If the sites -1 and 0 of the sublattice are both occupied by a spin up, the state is destroyed by $\tilde{H}(P)$: a quarter of the Hilbert space is a nullspace of $\tilde{H}(P)$. The nontrivial action of $\tilde{H}(P)$ in the remaining space corresponds to moving a configuration of N spins up on a lattice of $L = \log_2 \sqrt{D}$ sites with periodic boundary conditions through a two-site defect at -1 and 0 . If both spins at

-1 and 0 are down, $\tilde{H}(P)$ acts as a right or left global shift of the spins up by one site. If instead there is a single spin up at -1 or 0 , either that spin is moved to the other site or all spins up are globally shifted in the opposite direction. Importantly, once all spins up have passed across the defect, the relative distances between them are the same as in the initial configuration. This key observation allows us to represent *each* configuration as an effective particle propagating by a hopping Hamiltonian (with localised defects that can be seen as a deformation of the space), on an extended lattice of $L + N - 1$ sites. The mapping is described in the SM [47]. We find the energies to be parametrised as $E_P(k) = 4J \cos(k + P)$, where the momentum k of the effective particle and P satisfy

$$e^{i(L+N-1)k+iNP} = 1, \quad e^{iLP} = 1. \quad (12)$$

This mapping can also be exploited to compute the overlaps between the states and the matrix elements of the spin operators [47], providing therefore all the ingredients for the exact computation of the scaling profiles, such as the ones depicted in Figs 1 and 2.

For example, for odd x (for the general expression see SM [47]) the jamming condition (2) after the local spin flip can be written as (after the projective measurement there is instead an additional overall factor $1/3$)

$$\mathcal{P}_{\downarrow\downarrow}(x, t) = \frac{1}{L^2} \sum_N \sum_{\chi_N^{(1)}, \chi_N^{(2)}} \langle \varphi_0 | \chi_N^{(1)} \rangle \langle \chi_N^{(2)} | \varphi_0 \rangle \times \langle \chi_N^{(1)} | \downarrow \rangle \langle \downarrow | \chi_N^{(2)} \rangle e^{i \lceil \frac{x}{2} \rceil (P_1 - P_2) + it(E_{P_1}(k_1) - E_{P_2}(k_2))}. \quad (13)$$

Here, $\chi_N = (k; P, \dots)$ denotes the eigenstates and \dots stands for additional quantum numbers characterising the exponentially large sectors at fixed k and P . The sum excludes the jammed states, since the latter are destroyed by the observable. It turns out that the sum over the additional quantum numbers can be carried out analytically, and one can reduce the entire expression to a finite number of sums, which will be discussed in a more technical work still in preparation [48]. We only anticipate that a thorough analysis of (13) shows that, first, the terms with $N/L \sim 1/2$ contribute the most and, second, the asymptotic behaviour is determined by some singular points of the averaged matrix elements of the observable (the projector on two neighbouring spins down).

Numerical simulations. Apart from allowing for analytical investigation, our effective sublattice description of time evolution has also some numerical advantages. First, it almost doubles the system size accessible to exact diagonalisation techniques. In particular, systems with 26 spins can be simulated in a reasonable time with an ordinary laptop. As a matter of fact, it is also possible to perform semi-analytical calculations after having reduced expressions like (13) to finite numbers of sums. In that way it is possible to reach total system sizes of up

to ~ 60 sites ($L \sim 30$) in few days of single-processor computational time (the numerical effort is expected to scale as $L^{5.5} - L^6$). Our main numerical checks have been however based on DMRG algorithms, which describe the dynamics under investigation much more efficiently.

Profiles. We observe that, at large times, the numerical data are in excellent agreement with two ballistic-scale conjectures (i.e., $f(x, t) \rightarrow f(\zeta = \frac{x}{t})$)

$$t \mathcal{P}_{\downarrow\downarrow}(\zeta) \approx \frac{a}{\sqrt{1 - (\frac{\zeta}{v_{\pm}})^2}}, \quad \langle \sigma^y \rangle_{\zeta} \approx b \sqrt{1 - (\frac{\zeta}{v_{\pm}})^2}, \quad (14)$$

with $v_{\pm} = \pm 16J/3$, and whose assessment of validity is still in progress [48]. The constant prefactors in the scaling functions are well approximated by $a \approx 0.06$ and $b \approx 0.24$. These conjectures are consistent with the prediction for the maximal velocity of quasiparticle excitations on top of a jammed state

$$v_{\pm}[|\Phi\rangle] = \pm 8J / (1 + \frac{2}{L} \langle \Phi | S^z | \Phi \rangle), \quad (15)$$

which was derived in Ref. [49].

Can Alice recover the local state? After a time t , the reduced density matrix of Alice's site, assumed to be at an odd distance $x+1$ from Bob's past blind measurement at site -1 , reads

$$\rho_{\text{Alice}} = (\mathbb{1} + \vec{p}_{x,t} \cdot \vec{\sigma}) / 2, \quad (16)$$

with

$$\vec{p}_{x,t} = \frac{1}{3} \left(\langle \sigma^x \rangle_{\zeta} - 2 \cos \frac{\pi x}{n}, \langle \sigma^y \rangle_{\zeta} + 2 \sin \frac{\pi x}{n}, 0 \right). \quad (17)$$

Here $\zeta = x/t$, and the expectation values refer to the dynamics after the local spin flip — see Fig. 2. For ζ in the light-cone \vec{p} is slightly tilted from the initial (pre-measurement) direction, the tilt itself depending on Bob's position. As far as we can see, this makes it impossible for Alice to fully recover the information she had without Bob's measurement.

Summary. We addressed the question of how a local measurement in a jammed state of an interacting quantum system affects the late-time dynamics of distant local observables. The measurement triggers a ballistic dynamics in which jamming is locally restored but the profile of observables remains irremediably affected by the perturbation. Arguably, this prevents the full recovery of locally damaged information in the wing-flap protocol, which is instead expected quite generally [38].

Our work gives rise to several questions. Firstly, the precise mechanism that drives the reshaping of spin profiles after a local projective measurement is yet to be unveiled. We hope to resolve this issue in the ongoing analytical investigation [48]. The second question is that of repeated projective measurements, recently identified as the cause of dynamical phase transition in certain quantum many-body systems [50–53]. Their effects on the observables, as well as on the restoration of jamming pose

an intriguing open problem that could be investigated in the dual folded XXZ model even analytically.

Acknowledgements. We thank Viktor Eisler for useful discussions. This work was supported by the European Research Council under the Starting Grant No. 805252 LoCoMacro.

* maurizio.fagotti@universite-paris-saclay.fr

- [1] D. Jaksch and P. Zoller, The cold atom hubbard toolbox, *Annals of Physics* **315**, 52 (2005), special Issue.
- [2] I. Bloch, J. Dalibard, and S. Nascimbène, Quantum simulations with ultracold quantum gases, *Nature Physics* **8**, 267 (2012).
- [3] J. T. Barreiro *et al.*, An open-system quantum simulator with trapped ions, *Nature* **470**, 486 (2011).
- [4] T. R. Tan *et al.*, Multi-element logic gates for trapped-ion qubits, *Nature* **528**, 380 (2015).
- [5] H. Bernien, S. Schwartz, A. Keesling, H. Levine, A. Omran, H. Pichler, S. Choi, A. S. Zibrov, M. Endres, M. Greiner, V. Vuletić, and M. D. Lukin, Probing many-body dynamics on a 51-atom quantum simulator, *Nature* **551**, 579 (2017).
- [6] J. Zhang *et al.*, Observation of a many-body dynamical phase transition with a 53-qubit quantum simulator, *Nature* **551**, 601 (2017).
- [7] F. Arute *et al.*, Quantum supremacy using a programmable superconducting processor, *Nature* **574**, 505 (2019).
- [8] S. Ebadi, T. T. Wang, H. Levine, A. Keesling, G. Semeghini, A. Omran, D. Bluvstein, R. Samajdar, H. Pichler, W. W. Ho, S. Choi, S. Sachdev, M. Greiner, V. Vuletić, and M. D. Lukin, Quantum phases of matter on a 256-atom programmable quantum simulator, *Nature* **595**, 227 (2021).
- [9] I. Buluta and F. Nori, Quantum simulators, *Science* **326**, 108 (2009).
- [10] M. Schlosshauer, Quantum decoherence, *Physics Reports* **831**, 1 (2019), quantum decoherence.
- [11] V. Gritsev and A. Polkovnikov, Integrable Floquet dynamics, *SciPost Phys.* **2**, 021 (2017).
- [12] M. Vanicat, L. Zadnik, and T. Prosen, Integrable trotterization: Local conservation laws and boundary driving, *Phys. Rev. Lett.* **121**, 030606 (2018).
- [13] M. Ljubotina, L. Zadnik, and T. Prosen, Ballistic spin transport in a periodically driven integrable quantum system, *Phys. Rev. Lett.* **122**, 150605 (2019).
- [14] L. Sá, P. Ribeiro, and T. c. v. Prosen, Integrable nonunitary open quantum circuits, *Phys. Rev. B* **103**, 115132 (2021).
- [15] B. Bertini, P. Kos, and T. c. v. Prosen, Exact spectral form factor in a minimal model of many-body quantum chaos, *Phys. Rev. Lett.* **121**, 264101 (2018).
- [16] A. Nahum, J. Ruhman, S. Vijay, and J. Haah, Quantum entanglement growth under random unitary dynamics, *Phys. Rev. X* **7**, 031016 (2017).
- [17] A. Chan, A. De Luca, and J. T. Chalker, Solution of a minimal model for many-body quantum chaos, *Phys. Rev. X* **8**, 041019 (2018).
- [18] C. W. von Keyserlingk, T. Rakovszky, F. Pollmann, and S. L. Sondhi, Operator hydrodynamics, otocs, and entanglement growth in systems without conservation laws, *Phys. Rev. X* **8**, 021013 (2018).
- [19] V. Khemani, A. Vishwanath, and D. A. Huse, Operator spreading and the emergence of dissipative hydrodynamics under unitary evolution with conservation laws, *Phys. Rev. X* **8**, 031057 (2018).
- [20] J. Bensa and M. Žnidarič, Fastest local entanglement scrambler, multistage thermalization, and a non-hermitian phantom, *Phys. Rev. X* **11**, 031019 (2021).
- [21] I. L. Aleiner, Bethe ansatz solutions for certain periodic quantum circuits (2021), arXiv:2107.05715 [cond-mat.mes-hall].
- [22] P. W. Claeys, J. Herzog-Arbeitman, and A. Lamacraft, Correlations and commuting transfer matrices in integrable unitary circuits (2021), arXiv:2106.00640 [quant-ph].
- [23] V. Alba, J. Dubail, and M. Medenjak, Operator entanglement in interacting integrable quantum systems: The case of the rule 54 chain, *Phys. Rev. Lett.* **122**, 250603 (2019).
- [24] K. Klobas, B. Bertini, and L. Piroli, Exact thermalization dynamics in the “rule 54” quantum cellular automaton, *Phys. Rev. Lett.* **126**, 160602 (2021).
- [25] Y. Salathé *et al.*, Digital quantum simulation of spin models with circuit quantum electrodynamics, *Phys. Rev. X* **5**, 021027 (2015).
- [26] C. Neill *et al.*, Accurately computing the electronic properties of a quantum ring, *Nature* **594**, 508 (2021).
- [27] P. Calabrese, F. H. L. Essler, and G. Mussardo, Special issue on quantum integrability in out of equilibrium systems, *Journal of Statistical Mechanics: Theory and Experiment* **2016**, 064001 (2016).
- [28] B. Bertini and M. Fagotti, Determination of the nonequilibrium steady state emerging from a defect, *Phys. Rev. Lett.* **117**, 130402 (2016).
- [29] O. A. Castro-Alvaredo, B. Doyon, and T. Yoshimura, Emergent hydrodynamics in integrable quantum systems out of equilibrium, *Phys. Rev. X* **6**, 041065 (2016).
- [30] B. Bertini, M. Collura, J. De Nardis, and M. Fagotti, Transport in out-of-equilibrium XXZ chains: Exact profiles of charges and currents, *Phys. Rev. Lett.* **117**, 207201 (2016).
- [31] L. Piroli, J. De Nardis, M. Collura, B. Bertini, and M. Fagotti, Transport in out-of-equilibrium xxz chains: Nonballistic behavior and correlation functions, *Phys. Rev. B* **96**, 115124 (2017).
- [32] V. Eisler and F. Maislinger, Front dynamics in the XY chain after local excitations, *SciPost Phys.* **8**, 037 (2020).
- [33] M. Gruber and V. Eisler, Entanglement spreading after local fermionic excitations in the XXZ chain, *SciPost Phys.* **10**, 005 (2021).
- [34] V. Zauner, M. Ganahl, H. Evertz, and T. Nishino, Time evolution within a comoving window: Scaling of signal fronts and magnetization plateaus after a local quench in quantum spin chains, *J. Phys.: Condens. Matter* **27**, 425602 (2015).
- [35] V. Eisler, F. Maislinger, and H. G. Evertz, Universal front propagation in the quantum Ising chain with domain-wall initial states, *SciPost Phys.* **1**, 014 (2016).
- [36] V. Eisler and F. Maislinger, Hydrodynamical phase transition for domain-wall melting in the XY chain, *Phys. Rev. B* **98**, 161117(R) (2018).
- [37] M. Campisi and J. Goold, Thermodynamics of quantum information scrambling, *Phys. Rev. E* **95**, 062127 (2017).

- [38] B. Yan and N. A. Sinitsyn, Recovery of damaged information and the out-of-time-ordered correlators, *Phys. Rev. Lett.* **125**, 040605 (2020).
- [39] M. Gluza, J. Eisert, and T. Farrelly, Equilibration towards generalized gibbs ensembles in non-interacting theories, *SciPost Phys.* **7**, 038 (2019).
- [40] V. Alba, B. Bertini, M. Fagotti, L. Piroli, and P. Ruggiero, Generalized-Hydrodynamic approach to Inhomogeneous Quenches: Correlations, Entanglement and Quantum Effects, arXiv e-prints , arXiv:2104.00656 (2021), arXiv:2104.00656 [cond-mat.stat-mech].
- [41] L. Zadnik and M. Fagotti, The Folded Spin-1/2 XXZ Model: I. Diagonalisation, Jamming, and Ground State Properties, *SciPost Phys. Core* **4**, 10 (2021).
- [42] R. Z. Bariev, Integrable spin chain with two- and three-particle interactions, *Journal of Physics A: Mathematical and General* **24**, L549 (1991).
- [43] B. Pozsgay, T. Gombor, A. Hutsalyuk, Y. Jiang, L. Pristyaák, and E. Vernier, An integrable spin chain with hilbert space fragmentation and solvable real time dynamics (2021), arXiv:2105.02252.
- [44] G. I. Menon, M. Barma, and D. Dhar, Conservation laws and integrability of a one-dimensional model of diffusing dimers, *Journal of Statistical Physics* **86**, 1237 (1997).
- [45] Z.-C. Yang, F. Liu, A. V. Gorshkov, and T. Iadecola, Hilbert-space fragmentation from strict confinement, *Phys. Rev. Lett.* **124**, 207602 (2020).
- [46] M. Fagotti, On conservation laws, relaxation and pre-relaxation after a quantum quench, *Journal of Statistical Mechanics: Theory and Experiment* **2014**, P03016 (2014).
- [47] Supplementary material.
- [48] L. Zadnik and M. Fagotti, In preparation.
- [49] L. Zadnik, K. Bidzhiev, and M. Fagotti, The Folded Spin-1/2 XXZ Model: II. Thermodynamics and Hydrodynamics with a Minimal Set of Charges, *SciPost Phys.* **10**, 99 (2021).
- [50] Y. Li, X. Chen, and M. P. A. Fisher, Quantum zeno effect and the many-body entanglement transition, *Phys. Rev. B* **98**, 205136 (2018).
- [51] A. Chan, R. M. Nandkishore, M. Pretko, and G. Smith, Unitary-projective entanglement dynamics, *Phys. Rev. B* **99**, 224307 (2019).
- [52] B. Skinner, J. Ruhman, and A. Nahum, Measurement-induced phase transitions in the dynamics of entanglement, *Phys. Rev. X* **9**, 031009 (2019).
- [53] T. Minato, K. Sugimoto, T. Kuwahara, and K. Saito, Fate of measurement-induced phase transition in long-range interactions (2021), arXiv:2104.09118 [quant-ph].

Supplementary material for
“Macroscopic effects of localised measurements in jammed states of quantum spin chains”

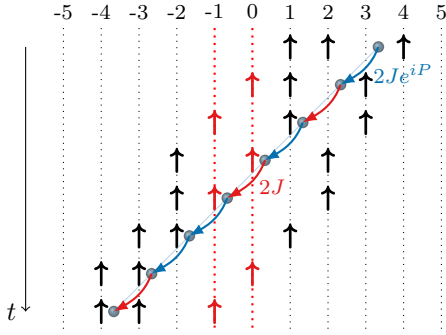
Kemal Bidzhiev¹, Maurizio Fagotti¹, Lenart Zadnik¹
¹ *Université Paris-Saclay, CNRS, LPTMS, 91405, Orsay, France*

The effective dynamics generated by $\tilde{H}(P)$

Here we describe the idea behind the diagonalisation of the effective Hamiltonian $\tilde{H}(P)$ from Eq. (11) of the main text. Detailed method will be presented in a separate publication [48]. Consider a configuration of N spins up; the effective Hamiltonian

$$\tilde{H}(P) = JK_{-1,0} + Je^{-iP}\Pi(\mathbb{1} - \sigma_{-1}^z) + Je^{iP}\Pi^{-1}(\mathbb{1} - \sigma_0^z) \quad (\text{S.1})$$

maps it into a superposition of identical configurations shifted by one site to the right (left), with a phase e^{-iP} (resp. e^{iP}). Repeated action of $\tilde{H}(P)$ propagates configuration in this manner until a spin up comes onto position -1 (or 0). The term $JK_{-1,0}$ then kicks in: the spin up jumps to position 0 (resp. -1) without acquiring a phase, while the rest of spins up retain their positions. Here is an example of nontrivial microscopic dynamics considering only the part of a superposition that moves in one direction:



For the coordinate of the effective particle (in blue) we have chosen a shifted centre-of-mass position

$$X(\underline{\ell}) = \frac{1}{N} \sum_{j=1}^N \ell_j + \frac{N-1}{2N} (N - 2N_-). \quad (\text{S.2})$$

Here ℓ_j are positions of spins up, N their total number, and N_- denotes the number of cases $\ell_j < 0$. The second term in (S.2) ensures that $X(\underline{\ell})$ changes by 1 even if only one of the spins up jumps between the sites -1 and 0 , while the rest of spins up retain their positions (the corresponding hopping of the effective particle is represented by the red curved arrows in the above diagram). The system is thus described by a hopping Hamiltonian on the lattice $\Lambda = X[\underline{\ell}] + \mathbb{Z}$ with defects accounting for the change in the coupling constants whenever a spin up jumps between the sites -1 and 0 (in red).

The defects can be removed via a unitary transformation, which leads to a hopping model with single-particle energy levels

$$E_P(k) = 4J \cos(k + P), \quad (\text{S.3})$$

where k denotes the momentum of the effective particle. The eigenstates of the effective Hamiltonian (11) are now parametrised as $|k; P, \underline{d}\rangle$, where \underline{d} is a collection of distances between subsequent spins up, defined so as to be preserved by the dynamics:

$$d_j = \ell_{j+1} - \ell_j - 1 + \theta(\ell_{j+1} < 0) - \theta(\ell_j < 0). \quad (\text{S.4})$$

For a finite sublattice size $L = \log_2 \sqrt{D}$ one needs to consider periodic boundary conditions, where k and P are instead quantised according to

$$e^{iLP} = 1, \quad e^{i(L+N-1)k+iNP} = 1. \quad (\text{S.5})$$

Quantisation of P follows from the momentum P being associated with a shift operator Π on the sublattice. The factor e^{iNP} in the quantisation condition for k is a result of the unitary transformation that removes the N defects and effectively adds a phase to each hopping process caused by the defect. Factor $e^{i(L+N-1)k}$ comes from the lag acquired by the configuration w.r.t. to the position of the effective particle, when the latter traverses the system. Each time a spin up jumps from 0 to -1 , the right-most spin up remains fixed, except if it itself jumps between these two sites. The total acquired lag is therefore $N-1$ sites, so the configuration needs $L+N-1$ steps before returning to its initial position.

As a proof of concept, Fig. S1(a) shows the comparison between the DMRG-based algorithm and exact diagonalisation of Hamiltonians $\tilde{H}(P)$.

Jamming condition $\mathcal{P}_{\downarrow\downarrow}(x, t)$

In this Section we describe the ingredients for the computation of the local jamming condition $\mathcal{P}_{\downarrow\downarrow}(x, t) = \frac{1}{4} \langle \Psi(t) | (\mathbb{1} - \sigma_x^z) (\mathbb{1} - \sigma_{x+1}^z) | \Psi(t) \rangle$ in Eq. (13) of the main text. Representation

$$|\Psi(t)\rangle = \sum_n (\sigma_n^x |\uparrow \dots \uparrow\rangle)_o \otimes |\varphi_n(t)\rangle_e \quad (\text{S.6})$$

of the wave function is useful to reduce the computation to the sublattice of even sites, where the condition becomes

$$\mathcal{P}_{\downarrow\downarrow} = \frac{1}{2} \begin{cases} \langle \varphi_{\frac{x}{2}+1}(t) | \mathbb{1} - \sigma_{\frac{x}{2}}^z | \varphi_{\frac{x}{2}+1}(t) \rangle & x \text{ even,} \\ \langle \varphi_{\frac{x+1}{2}}(t) | \mathbb{1} - \sigma_{\frac{x+1}{2}}^z | \varphi_{\frac{x+1}{2}}(t) \rangle & x \text{ odd.} \end{cases} \quad (\text{S.7})$$

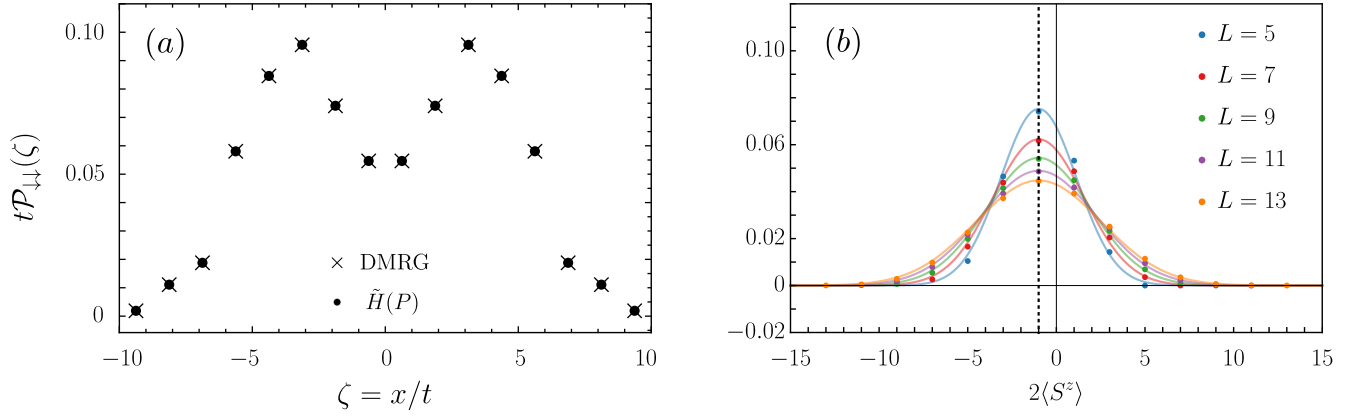


FIG. S1. Panel (a) shows the profile $t\mathcal{P}_{\downarrow\downarrow}(x, t)$ at $t = 0.8$, for $L = 13$ (a chain of 26 spins), computed with a DMRG-based algorithm and exact diagonalisation of the effective Hamiltonians (S.1). Panel (b) shows contributions to $\mathcal{P}_{\downarrow\downarrow}$ coming from summing the elements with given N (and hence $\langle S^z \rangle$) at $x = 0$ and $t = 1/2$ for the sublattice sizes $5 \leq L \leq 13$. Data are fitted with Gaussian curves centered around the sublattice magnetisation $2\langle S^z \rangle = 2N - L = -1$. The full width at half maximum scales sublinearly with the sublattice size. The term with the highest contribution is $N = (L - 1)/2$.

The operators on the right-hand side act on the state of the sublattice – their indices have been changed ac-

ordingly. Using Eqs (9), (10) of the main text, we then obtain

$$\begin{aligned} \mathcal{P}_{\downarrow\downarrow} = & \frac{1}{L^2} \sum_N \sum_{\underline{d}_N^{(1)}, \underline{d}_N^{(2)}} \sum_{\substack{P_1, P_2 \\ e^{iLP=1}}} \sum_{\substack{k_1, k_2 \\ e^{i(L+N-1)k+iNP=1}}} e^{i\left(\frac{x}{2} + \frac{3+(-1)^x}{4}\right)(P_1 - P_2)} e^{i4Jt(\cos(k_1 + P_1) - \cos(k_2 + P_2))} \times \\ & \times \langle \varphi_0 | k_1; P_1, \underline{d}_N^{(1)} \rangle \langle k_1; P_1, \underline{d}_N^{(1)} | \frac{\mathbb{1} - \sigma^z_{-[1+(-1)^x]/2}}{2} | k_2; P_2, \underline{d}_N^{(2)} \rangle \langle k_2; P_2, \underline{d}_N^{(2)} | \varphi_0 \rangle. \end{aligned} \quad (\text{S.8})$$

The matrix element and the overlaps between the wave functions can be computed exactly by employing the mapping between a configuration of spins up and an effective particle [48]. Here we only report the resulting formulas for the case $|\varphi_0\rangle = |\leftarrow \dots \leftarrow\rangle$ (i.e. after a local measurement in the state $|\mathcal{L}_1\rangle$). For $k_1 \neq k_2$ they read

$$\begin{aligned} \langle \leftarrow \dots \leftarrow | k; P, \underline{d}_N \rangle &= \frac{1 - e^{iP}}{e^{ik} - 1} \sum_{\ell=1}^N \frac{e^{i(2\ell-1-2N+\sum_{n=N+1-\ell}^{N-1} d_n)k} e^{i(\ell-1)P}}{\sqrt{2^L(L+N-1)}}, \\ \langle k_1; P_1 \underline{d}_N | \frac{\mathbb{1} - \sigma^z}{2} | k_2; P_2, \underline{d}_N \rangle &= \frac{1 - e^{i(P_2 - P_1)} e^{i(k_2 - k_1)}}{e^{i(k_2 - k_1)} - 1} \sum_{\ell=0}^{N-1} \frac{e^{i(2\ell+1-2N+\sum_{n=N-\ell}^{N-1} d_n)(k_2 - k_1) + i\ell(P_2 - P_1)}}{L + N - 1}, \\ \langle k_1; P_1, \underline{d}_N | \frac{\mathbb{1} - \sigma^z}{2} | k_2; P_2, \underline{d}_N \rangle &= e^{i(k_1 - k_2)} \langle k_1; P_1 \underline{d}_N | \frac{\mathbb{1} - \sigma^z}{2} | k_2; P_2, \underline{d}_N \rangle, \end{aligned} \quad (\text{S.9})$$

whereas the limit $k_1 = k_2$ has to be performed carefully, taking the quantisation conditions (S.5) into account. We point out that the numerical computation of the fixed- N terms in (S.8) for small system sizes (via exact diagonalisation) suggests that the main contribution to the jamming condition $\mathcal{P}_{\downarrow\downarrow}(x, t)$ at fixed x and t comes from the terms with $N \sim L/2$ – see Fig. S1(b). This numerical observation can be proved analytically and holds for any sublattice size L [48].

Reduced density matrices

The purpose of this Section is to explain Bob's reduced density matrices. Bob performs a blind projective measurement on one of the spins up in a factorised state. Suppose that the axis of the measurement is fixed. It can be obtained by rotating the z -axis by an angle $\phi \in [0, \pi)$ around the xy -plane unit vector $\hat{n}_\phi = (\cos \phi, \sin \phi, 0)$, parametrised by $\varphi \in [0, 2\pi)$. Had Bob read off the result of the measurement, the spin would have collapsed into

the state

$$\rho(\Phi, \varphi) = e^{i\frac{\phi}{2}\hat{n}_\varphi\cdot\vec{\sigma}} |\uparrow\rangle\langle\uparrow| e^{-i\frac{\phi}{2}\hat{n}_\varphi\cdot\vec{\sigma}}. \quad (\text{S.10})$$

In our protocol, described in the main text, the measurement is instead blind: Bob does not read off its result. Hence, due to a classical uncertainty, the state after the measurement is computed as an average w.r.t. the Haar

measure:

$$\begin{aligned} \rho_{\text{Bob}} &= \int_0^{2\pi} \frac{d\varphi}{2\pi} \int_0^\pi \frac{d\phi}{\pi} \rho(\phi, \varphi) \left(\frac{\pi}{2} \cos \frac{\phi}{2} \right) = \\ &= \frac{2}{3} |\uparrow\rangle\langle\uparrow| + \frac{1}{3} |\downarrow\rangle\langle\downarrow|. \end{aligned} \quad (\text{S.11})$$

The weight $\frac{\pi}{2} \cos \frac{\phi}{2}$ in the integral is the probability for the nonzero projection of the spin up onto the measurement axis.